https://dx.doi.org/10.1016/j.clay.2023.107237

Physicochemical properties of clayey deposits slurry treated by lime-activated ISSA and GGBS considering seawater salinity effect

Zhao SUN[2,3], Wen-Bo CHEN[*1], Run-Dong ZHAO[2], Jiang-Shan LI[4], Zhen-Yu YIN[2], Jian-Hua YIN[2], Yong-Gui CHEN[3]

[1]*College of Civil and Transportation Engineering, Shenzhen University, Shenzhen, Guangdong, China.*

[2]*Department of civil and environmental engineering, The Hong Kong Polytechnic University, Hung Hom, Kowloon, Hong Kong, China.*

[3] *Department of Geotechnical Engineering, School of Civil Engineering, Tongji University, Shanghai, China.*

[4]*Institute of Rock and Soil Mechanics, Chinese Academy of Science, Wuhan 430071, China.*

Corresponding author: Wenbo CHEN

Email : wenbochen@polyu.edu.hk

Phone : 852-3400 8075

Abstract

This study sheds light on the engineering and environmental performance of lime-activated incinerated sewage sludge ash (ISSA) and ground granulated blast furnace slag (GGBS) treated Hong Kong marine deposits (HKMD) slurry by stabilisation/solidification (S/S) technology, which is proposed using as fill material in reclamation projects. The S/S performance of the treated HKMD with distilled water and seawater under different salinities was investigated. The results show that seawater could help S/S treated HKMD gain strength by using activated industrial wastes (ISSA and GGBS). The hydration and pozzolanic reactions between ISSA, GGBS, CaO and clayey compositions in HKMD make contributions to the strength development, porosity decrease and heavy metals stabilization, which is supported by the characterization analysis including thermo-gravimetric (TG) analysis, mercury intrusion porosimetry (MIP) tests, nitrogen adsorption/desorption isotherms (NAI), scanning electron microscopy coupled with energy-dispersive spectrometry (SEM-EDS) and the leaching test of toxicity characteristic leaching procedure (TCLP). Seawater of 1.8% salinity (18 g/kg) is better than the distilled water and seawater of 3.6% salinity as a substrate solution in the S/S treated HKMD, because of the highest unconfined compressive strength and lowest porosity in the treated samples. The highest pH may account for its highest strength under the 1.8% salinity conditions. The S/S process could effectively stabilize the contaminants regardless of the curing time and the salinity of the mixing solution, and the leachates from the stabilized HKMD are environmentally safe and meet the requirement of standard in Hong Kong on the recycling treated soil. Therefore, recycling wastes—ISSA and GGBS with lime can be used as an appealing binder to stabilise/solidify marine deposits as environmental-friendly reusable materials in reclamation projects.

Keywords: Stabilisation/solidification, Hong Kong marine deposits, Industrial wastes reuse, Salinity of seawater, Metal leachability

1 Introduction

Soft soils have been used as fill material in land reclamation projects in mainland China and Singapore. However, most of the newly blow-filled soft soil are clayey soils possessing high water content, low permeability and low strength. In Hong Kong, dredged marine sediments are produced 29 Mm^3 per year and approximately 1200 tonnes per day of dewatered sewage sludge are produced converting into incinerated sewage sludge ash (ISSA) after incineration (Zhou et al., 2021a). It would take up many landfills to dispose of both dredged marine sediments and ISSA resulting in an urgent issue to identify suitable disposal sites. The current study sheds light on possible beneficial use of industrial wastes--ISSA and ground granulated blast furnace slag (GGBS) to treat Hong Kong marine deposits (HKMD) slurry to produce fill material in reclamation project. In order to achieve this goal, there are two basic requirements: 1) the treated HKMD using ISSA and GGBS gains competent bearing capacity; 2) the leachability of contaminants from the treated HKMD meets the reuse standards of treated soil, which is more stringent than that in standard of landfill soil (HK EPD 2011). Since industrial wastes (e.g., ISSA) contain a variety of heavy metals, and many types of dredged sediments are classified as unacceptably contaminated in Hong Kong (Wang et al., 2015). Thus, the potential environmental risks exist. While stabilisation/solidification (S/S) technology can meet both of the requirements in improving the physical and mechanical properties of treated soft soil (Lofrano et al., 2017; Li et al., 2019) and reducing the heavy metals dissolution, migration and leaching toxicity in soil environment (Malviya and Chaudhary, 2006).

In recent years, the development of new sustainable S/S materials is sought and of global interest for the immobilization of heavy metals in contaminated soils (Emmanuel et al., 2020). In this work, the lime-activated ISSA and GGBS were adopted as the binders in the S/S treatment of HKMD with seawater as matrix solution. It makes more sense to use activated industrial wastes as an alternative binder material to cement from both engineering and environmental point of view. Numerous previous works have studied that lime can increase soil pH, promote precipitation of metal oxides, hydroxides or carbonates and decrease heavy metal solubility (Castaldi et al., 2005; Chen et al., 2021; Gong et al., 2021; Xu et al., 2021). Additionally, a large amount of heavy metals would have a negative impact on the mechanical properties of geomaterials (Zhang et al., 2022a). It is found that high pH in the system is conducive to

immobilizing toxic metals by adsorption, precipitation and ion exchange reactions (Malviya and Chaudhary, 2006). ISSA as a stabilisation agent was found effectively in S/S soft soil treatment (Chen and Lin, 2009; Li et al., 2019; Zhou et al., 2020; Jagaba et al., 2019). Zhou et al. (2020) found that a moderate pozzolanic activity in the ISSA - soft soil system. Another industrial waste-GGBS can help the soft soil to improve the strength (Zentar et al., 2012; Celik and Nalbantoglu, 2013; Cai et al. 2022; Yi et al., 2015; Song et al., 2023). Furthermore, the stabilizing effect of activated GGBS as a binder on heavy-metal contaminated soils has been confirmed (Jin et al., 2016; Wu et al., 2018). Sun et al. (2023a) investigated the treated HKMD slurry by the lime, activated ISSA and GGBS with dosage of 30% by dry weight of HKMD. It was found that the hydration products such as ettringite (AFt), Friedel's salt (F's salt) and calcium/magnesium silicate hydrate (C/M-S-H) and fill into the pores of the treated soil and interlock the particles in the mixture, which increases the soil strength. Additionally, seawater was reported playing a positive role as matrix solution in the S/S treatment of HKMD (Sun et al., 2023b), which is in agreement with the findings from Ashraf et al. (2022) that due to the alkalinity (pH 8.2) of seawater, it could act as an activator for the calcined clay-portlandite mixtures.

Previous research has confirmed that the factors, such as the binder material (Zhou et al., 2022), the binder content (Deng et al., 2015; Li and Yi, 2023), the water content (Lang et al., 2021), the soil type (Deng et al., 2015; Zhou et al., 2022), and chemical compositions of mixing solution (Zhao et al., 2021; Sun et al., 2023b), etc., have impacts on the property of treated soil. Recently, studies have shown that the change of pore water salinity can also change the inherent properties of reconstituted clay (Song et al. 2017; Deng et al. 2018; Sun et al., 2020); but, the change of physiochemical properties of stabilized marine clay due to seawater salinity has rarely been evaluated (Bayesteh and Bayat, 2021). Some researchers investigated on the effect of salinity on the engineering properties of cement mixing soils or dredged materials (e.g., Horpibulsuk et al. 2012; Khoshsirat et al., 2019; Monsif et al., 2020). Horpibulsuk et al. (2012) studied the unconfined compressive strength (UCS) of cement stabilization of soft saline clays and found that the presence of salt (95.5% of NaCl) not only reduces the attraction and bonding strength between clay particles, but also adversely affects the hydration of cement. Zhang et al. (2014) indicated that a high salinity of NaCl has a detrimental effect on the UCS of cement stabilized clay. The findings in Monsif et al. (2020) presented the impact of salinity (by mixing NaCl) on the

strength of cement-treated Champlain Sea clay and found that the UCS of treated soil shows no obvious rule with the salinity increasing. Khoshsirat et al. (2019) pointed out that seawater salinity could control the UCS of cement-stabilized marine clay by affecting the microstructural configuration of the clay and the pozzolanic reaction. In addition, the UCS of treated soil also presents a trend of increasing first and then decreasing while the salinity increasing from low to high level. Zhou et al. (2021b) observed that the strength of the lime-ISSA paste with seawater was double higher than that of paste with freshwater at 28 curing days. However, these studies only examined the salinity of NaCl on the cement treated soil properties or focused on the phenomenon of cement treated soil strength affected by the seawater salinity. Sun et al. (2023b) attempted to analyse the effect of seawater components on the S/S mechanism of treated HKMD by lime-activated ISSA-GGBS. Nevertheless, the effect of seawater salinity on the S/S treated HKMD was not taken into account.

Thus, there is no conclusive finding about the effect of seawater salinity on the S/S performance of treated marine clay treated by materials other than cement. This study aims to evaluate the effect of seawater salinity on the stabilisation/solidification performance of HKMD by lime-activated industrial wastes from the aspects of engineering strength and environmental risk assessment. The objectives of this study are to reveal: a) the effect of seawater with different levels of salinity on the physical and mechanical property of the S/S HKMD; b) the microstructural property of the S/S HKMD affected by seawater salinity; c) the morphology of the neoformations and heavy metals in the S/S HKMD; d) the leaching behavior of heavy metal(loid)s including arsenic (As), cadmium (Cd), chromium (Cr), copper (Cu), zinc (Zn), nickel (Ni) and lead (Pb) from HKMD before and after S/S treatment. According to Huang et al. (2019), heavy metals such as As, Cu, Zn, Ni, Cd, Cr, Pb, etc., are enrich in Chinese contaminated soils. In particular, Cd is categorized as the most hazardous metal by the United States Environmental Protection Agency (Gong et al., 2021). Macroscopic tests were carried out to investigate the macro- performance of S/S treated HKMD. Thermo-gravimetric (TG) analysis, mercury intrusion porosimetry technique (MIP) tests, nitrogen adsorption/desorption isotherms (NAI) and scanning electron microscopy coupled with energy-dispersive spectrometry (SEM-EDS) were performed to analyse the S/S mechanism of the treated HKMD. Besides, the toxicity characteristic leaching method (TCLP) was used for the first time to evaluate the environmental risk of HKMD after S/S treatment.

2 Materials and Methodologies

2.1 Hong Kong marine deposits and binder materials

The dredging site for deposits collecting is near lamma island in Hong Kong. The basic parameters of dredged HKMD are listed in Table 1. Among them, the BET SSA is the specific surface area (SSA) calculated by Brunauer-Emmett-Teller (BET) method. The main compositions of the HKMD include kaolinite, muscovite, quartz, halite, albite and phillipsite with the specific content of 14.4%, 11%, 55%, 8.3%, 4%, 3.7%, respectively.

Table 1. Basic properties of Hong Kong marine deposits.

G_s	Plastic limit (%)	Liquid limit (%)	PI	BET SSA (m^2/g)	pH
2.525	33	50	17	12.94	7.54

The oxide compositions of ISSA, GGBS and lime detected by X-ray fluorescence (XRF, Rigaku Supermini 200) was described in Sun et al. (2023b). The particle size of HKMD, ISSA and GGBS was presented in Sun et al. (2023a). Seven heavy metals from the materials including As, Cd, Cr, Cu, Zn, Ni and Pb were investigated. As shown in Table 2, the leachability of these heavy metals from the raw HKMD, ISSA and GGBS does not exceed the Landfill Disposal Criteria for Contaminated Soil standard in Hong Kong (HK EPD 2011). While the theoretical value of the heavy metals in the treated soil as-mixed does not meet the On-site Reuse of Cement Stabilisation/Solidification Treated Soil standard (HK EPD 2011), especially for Cd, Cr, Pb and Zn. Thus, the environmental risk should be studied before the direct reuse of the treated HKMD.

Table 2. Heavy metals and their concentrations from marine deposits and the industrial wastes.

Materials	Heavy metal (loid)s (mg/kg)						
	As	Cd	Cr	Ni	Cu	Pb	Zn
HKMD	0.175	0.222	1.98	3.01	0.426	1.272	3.95
ISSA	5.9	0.84	2.02	2.38	25.56	0.78	23.94
GGBS	0.134	0.17	1.87	0.287	0.418	1.04	0.56

Raw mixture[#]	1.06	0.30	1.80	2.50	4.35	1.07	6.56

[#] The value of the heavy metal (loid)s in the mixture just mixed: $C^{\#}= C_{HKMD} \times 70\% + (C_{ISSA} \times 75\% + C_{GGBS} \times 25\%) \times 70\% \times 30\%$.

2.2 Testing methods

2.2.1 Sample preparation

Firstly, the dried ISSA and GGBS with a mass ratio of 3:1 was mixed. Then, the lime and ISSA-GGBS were mixed in a ratio of 3:7 to form the binder. Before sample preparation, the HKMD paste was adjusted to 110% water content with distilled water (DW) and seawater (SW) with salinity of 18 and 36 g/kg (1.8% and 3.6%). The compositions of seawater are shown in Table 3. The mixed binders were adopted with a dosage of 30% HKMD in dry weight. The cylindrical moulds of 100 mm in height and 50 mm in diameter were used to place the treated mud. The moulds were finally stored in a chamber with humidity of around 95 % and temperature at 20 ± 2 °C. The specific sample preparation process is shown in Fig. 1.

Fig. 1. Schematic diagram of sample preparation (Sun et al., 2023a).

Table 3. Compositions (in mg/L) of Red Sea salts used in this work

Compound	Cl	Na	Mg	S	Ca	K	C (inorg.)	Br

Concentration	18,772	10,691	1320	890	480	390	45	15

2.2.2 Property tests

The treated samples were dried in an oven at 105 °C for 24 h to determine their water contents. The specific gravity of materials was measured by a BELPycno L Gas Pycnometer (Microtrac MRB, Japan). The wax sealing method was used to measure the bulk density of S/S samples. All these results used for data analysis were the average of triplicates. The unconfined compression tests were conducted on the S/S HKMD samples by using a VJ-Tech Tri-Scan 50 compression machine.

2.2.3 Characterization tests

After curing, the specimens would be cut and frozen-dried for 48 h in a freeze-drier (Labconco Freezone 2.5 Plus). TG analysis (Netzsch STA 449F3) was carried out on S/S HKMD powder with the weight around 10 mg after the frozen-dried process. The temperature was increased from 40 to 900 °C at a rate of 10 °C /min in the TG tests. To prevent carbonation of S/S HKMD samples, the nitrogen gas was used with a flow rate of 50 mL/min during the heating. MIP tests were carried out on Autopore V 9600 from Micromeritics to measure the porosity and pore size distribution (PSD) of S/S treated HKMD. NAI method was adopted by using a TriStar II 3020 porosity and surface area analyzer (Micromeritics Instruments Corporation) to detect the treated material porosity in powder state. The morphology and elemental distribution of the S/S treated HKMD samples were observed by SEM with EDS on TESCAN VEGA 3 in the secondary electron (SE) mode.

2.2.4 Metal(loid)s leaching tests

TCLP test was adopted to determine the leachability of heavy metal(loid)s in the materials before and after the S/S treatment according to the EPA Method 1311 (US EPA 1992). The leachates were subjected to acid digestion by concentrated HNO_3 (68%). Then, the heavy metal concentrations of the leachates were measured by Inductively Coupled Plasma-Atomic Emission Spectroscopy (ICP-AES, PerkinElmer Optima 3300DV). Two or three measurements were conducted for each sample, and the average value was used in the analysis.

3 Results and analysis

3.1 Macro- property of treated material

3.1.1 Physical properties

The water content and void ratio of the treated HKMD samples with curing times are presented in Fig. 2. The true density and bulk density of treated HKMD are listed in Table 4. From Fig. 2(a), it is seen that the water content of the freshly mixed paste is around 84%. The reduction of water content with time is found in the treated samples. From the slope of the curves, it is obvious that the decrease of water content at the period of 0-28 days is most intense, which indicates the faster reaction speed in the system within this period. That is the S/S HKMD mixed with SW of 1.8% salinity have the highest reaction rate during the curing process. The external water content decrease should be due to the water consumption in the hydration and pozzolanic reactions generating new hydration products in the system, which is in agreement with the findings in Cai et al. (2022). Thus, the lowest water content in the mixture with seawater of 1.8% salinity suggests a high content of hydration products and a high content of absorbed water as well (Li et al., 2022).

The void ratio (e) of the S/S treated HKMD specimens at different curing time is drawn in Fig. 2 (b). It was calculated from the equation $e = G_s(1+ w)\rho_w/\rho$-1, in which G_s is the specific gravity with its value taken as true density in this work, w is the water content, ρ_w is the water density, and ρ is the bulk density of the S/S HKMD specimens. It is found that the calculated void ratio lies between 1.95 and 2 and decreases with the curing time generally. Therefore, it can be inferred that the voids in the bulk sample were gradually filled by hydration products (Li et al., 2022).

The true density and bulk density of treated HKMD after different curing periods are presented in Table 4. The true density of HKMD, GGBS and ISSA is 2.525, 2.69 and 2.68 g/cm^3, respectively. It is seen that the bulk density and true density of the samples mixed with three kinds of solution increase with time overall, and most of the true density are less than 2.525. It should be due to the hydration products (e.g., C-S-H), which has a lower density of about 2.25-2.35 g/cm^3 (Bernard et al., 2017). In addition, the true density increases with curing time, which may be partly because of the more absorbed water during

the reaction processes (Li et al., 2022), and partly because of the crystallization of amorphous products or the densification of the C-S-H or calcium aluminium silicate hydrate (C-A-S-H) over time (Avet et al., 2019).

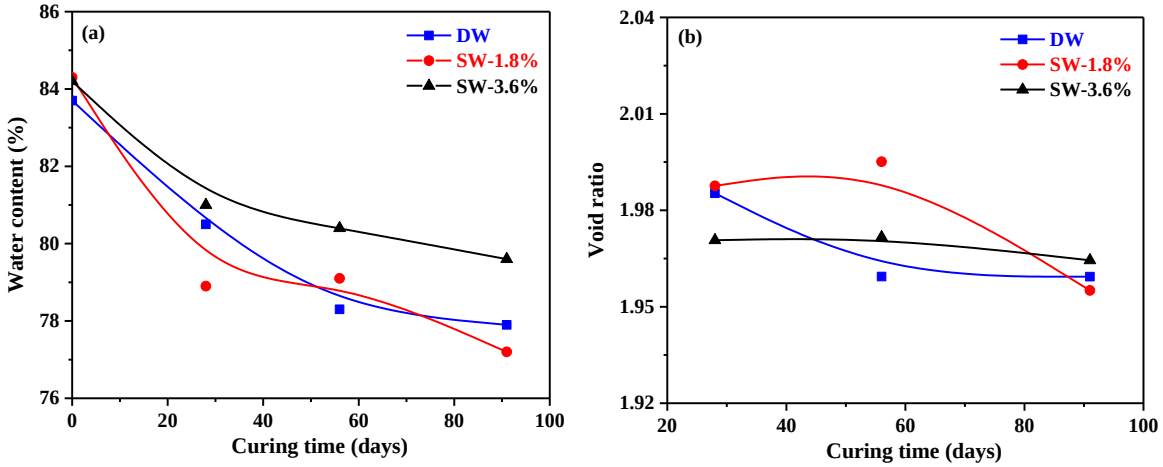

Fig. 2. The water content and void ratio of treated HKMD with curing time.

Table 4. The bulk density and true density of treated HKMD.

Density	Time (days)	DW	SW-1.8%	SW-3.6%
Bulk density	28	1.514	1.509	1.522
	56	1.512	1.508	1.520
	91	1.515	1.523	1.534
True density	28	2.504	2.52	2.498
	56	2.510	2.521	2.503
	91	2.520	2.539	2.532

3.1.2 Mechanical properties of treated samples

The mechanical properties of S/S HKMD samples with seawater of different levels of salinity are shown in Fig. 3, in which the results in treated samples mixed with SW of 3.6% salinity is referred to Sun et al. (2023b). From Fig. 3(a). It is seen that all the specimens gain their UCS, and the UCS increases with curing time. The samples mixed with seawater of 0, 1.8% and 3.6% salinity yield a maximum UCS at the 91st curing day, which is 1200, 1276 and 1001 kPa, respectively. At 56 days, the UCS of treated samples reaches more than 85% of that at 91 days under each solution conditions. While at 28 days, the UCS is around 62-68% of that at 91 days. In general, the UCS of samples with seawater of 1.8% salinity is higher than that of samples under the other two conditions. While the HKMD slurry at initial water content of 110% exhibits no strength at all, it demonstrates that the binders of ISSA- GGBS in this work

are effective in S/S treatment of HKMD. Additionally, the highest strength investigated from the 91-day curing samples suggests moderate reactions in the system (Zhou et al., 2022). The deformation modulus E_{50} of the treated HKMD calculated as the secant modulus at 50% of UCS is an important parameter reflecting the deformation resistance of geomaterials. According to Fig. 3(b), the E_{50} of S/S treated HKMD specimens with three mixing proportions are also increasing with time. It is presented that the modulus of the specimens with DW is higher than that of samples with SW solutions. The findings are in consistent with the investigations about the impact of salinity on the strength of cement-treated Champlain Sea clay by Monsif et al. (2020), which found that a high salinity such as 30.55 g/L has a negative impact on the soil strength.

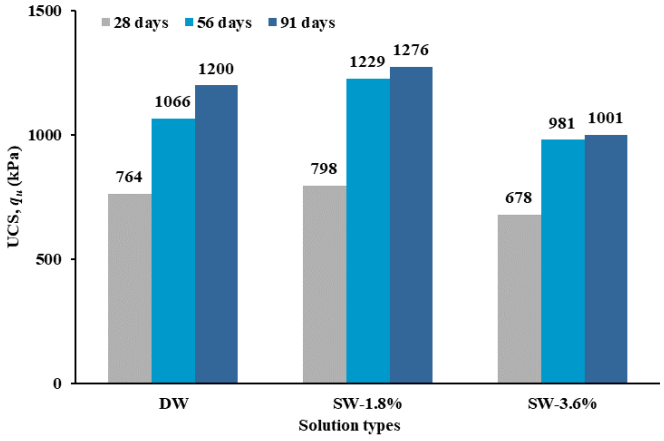

(a) UCS of treated samples

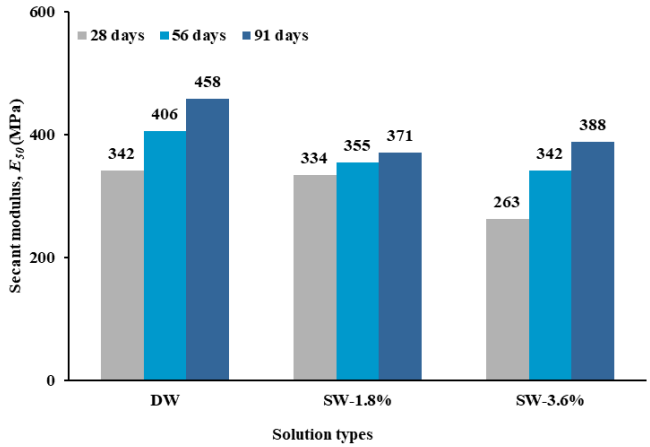

(b) Modulus of treated samples

Fig. 3. The mechanical properties of the treated HKMD samples.

3.2 TG analysis

The TG and DTG curves of raw HKMD and S/S treated HKMD are shown in Fig. 4 with the temperature ranging from 30-900 °C. The weight loss of each temperature period obtained from TG data are presented in Table 5. Among them the data of treated samples under the SW-3.6% salinity conditions are referred to Sun et al. (2023b). Firstly, from the TG and DTG curves of raw HKMD, it is obvious that the most weight loss occurs at temperature from 400 to 800 °C. The peak on the DTG curve from 400 to 500 °C should be contributed to the dehydroxylation in kaolinite (Avet and Scrivener, 2018). Additionally, the weight loss peaks at 500-700 °C represents the decomposition of illite (Húlan et al., 2015), and the peak at 700-800 °C is associated with the dehydroxylation in montmorillonite (Li et al., 2022).

After the S/S treatment of HKMD, the weight loss of the possible products in the complex system was analysed. It was reported that the mass loss at 40-280 °C is due to the loss of the poorly bound water in several hydration formations including AFt (Shen et al., 2017), C/M-S-H (Nied et al., 2016; Bernard et al., 2017) and part of F's salt (230-370 °C) (Zhou et al., 2021b). From Fig. 4, the water loss of AFt appears at 50-160 °C with the peak at around 100 °C in the treated soils (Avet and Scrivener 2018; Wang et al., 2004). The $Ca(OH)_2$ (CH) loss is considered from 370 to 600 °C (Alarcon-Ruiz et al., 2005; Wang et al., 2004; Li et al., 2019), and the decarbonation of $CaCO_3$ (CC) loss ranges from 600 to 720 °C (Prochon and Piotrowski, 2020; Lu and Poon, 2018; Scrivener et al., 2017; Sun et al., 2023b). The dihydroxylation of Ca–OH in C-S-H occurs from 300-600 °C, and that of Mg–OH in M-S-H is at 400-750 °C (Bernard et al., 2017, 2019). In addition, the weight loss occurs in silanol groups on M-S-H at 720-900 °C (Nied et al. 2016). The inner OH groups in the crystallized C/M-S-H such as the talc structure dehydroxylates at 750-1000 °C (Dumas et al., 2013; Gallucci et al., 2013; Bernard et al., 2019; Chakraborty et al., 2022). From Table 5, it shows that the weight loss between 400 and 600 °C is highest in all samples. Since the mass content of raw HKMD in the mixture is 70%, the maximum weight loss of HKMD in the treated samples is about 70% of that in raw HKMD, that is 3.37%, which is lower than the values in the treated material. It confirms the new products in the mixed system.

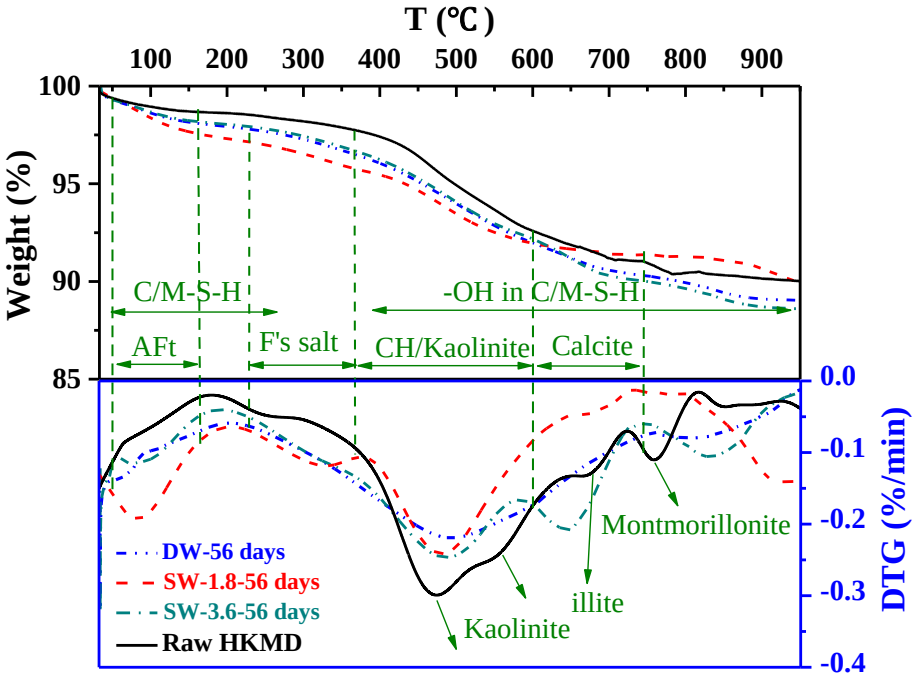

Fig. 4. TG and DTG curves of HKMD before and after treatment at 56 curing days.

Table 5. Weight loss of HKMD before and after treatment at 56 curing days.

Condition	Weight loss (% of original)					
	30-200 ℃	200-400 ℃	400-600 ℃	600-750 ℃	750-900 ℃	Total
HKMD*	0.969	0.844	3.373	1.155	0.554	6.896
DW	2.069	1.882	4.073	1.700	1.172	10.896
SW-1.8%	2.691	1.851	3.507	0.546	0.755	9.350
SW-3.6%	1.958	1.805	4.062	2.181	1.291	11.299

*Theory weight loss of HKMD in the treated samples is shown here, which is 70% that of the raw HKMD.

3.3 MIP analysis

The microstructure of the treated specimens at 56 curing days was detected by MIP tests with the PSD results shown in Fig. 5. The figure illustrates a unimodal PSD with a centre pore diameter of approximately 0.33 μm in the S/S samples, which suggests that the diameter of the largest pore group is approximately 0.33 μm (Sun et al., 2023b). The result is similar with the diameter of the largest pore group in the PSD of stabilized soils with metakaolin by 15% cement reported by Deng et al. (2015). The cumulative intrusion volume of the treated specimens at 56 days is also presented in Fig. 5(a), which is around 0.8 mL/g.

To better understand the PSD in HKMD samples after S/S treatment, the pores are classified to three groups: > 2 μm, 50 nm-2 μm and 5-50 nm. Because of the limitation of MIP method, the nano-pores (1-

5 nm) in C/M-S-H gels could not be detected, and thus the nano-pore volume. It was investigated by SEM observation with high magnification that the average size of inner pores of M-S-H aggregate is around 30 nm (Chiang et al., 2014; Tonelli et al., 2016). While that of C-S-H aggregate is more than 50 nm (Chiang et al., 2014). Thus, 50 nm was selected to distinguish the inner pore size of M-S-H and C-S-H aggregates. The diameter of 2 μm is a typical width of the cracks as estimated by SEM images of S/S treated HKMD using lime-activated ISSA-GGBS (Sun et al., 2023b). Thus, the biggest pore size group are assigned with size > 2 μm representing the cracks and air pores in the treated soil (Dewitte et al., 2022; Horpibulsuk et al., 2009).

Fig. 5(b) shows the pore volume percentage of the treated samples at curing age of 28 and 56 days. The pore group with diameter from 5 to 50 nm is mainly composed of gel pores, pores in the kaolinite particle from the deposits and pores in the M-S-H aggregates (Horpibulsuk et al., 2010; Tonelli et al., 2016; Yu et al., 2016; Dewitte et al., 2022). As the pores of 5-50 nm partly represent the inner pores in M-S-H aggregates, it is obvious that this part of pore volume fraction in S/S HKMD specimens increases with curing days, which confirms the increasing content of M-S-H products. Salinity effect on this part of pore volume is not obvious. The pore of diameter from 50 nm to 2 μm includes the inter-aggregate pores in kaolinite and C-S-H, and capillary pores (Dewitte et al., 2022; Yu et al., 2016; Zeng et al. 2012). The volume of pores with size from 50 nm to 2 μm in the S/S treated HKMD with three solutions is the largest. The volume of largest pore group (> 2 μm) increases with time in the samples with DW and SW of 1.8% salinity, which suggests the more cracks. It is in agreement with the opinion from Horpibulsuk et al. (2009) that after mixing clayey soil with cementious material, because of the physicochemical interaction in the mixture the formation of clusters would reduce the small pore (e.g. <0.1 μm) volume and increase the large pore (e.g. > 0.1 μm) volume. Then, it would result in the increase of the dry unit weight, which is in agreement with our density results listed in Table 4. Moreover, the clusters, such as C-S-H particles, would harden and shrink during the curing process of transforming from a gel to a crystalline state, which will also reduce the small pores and increase the large pores resulting in more air pores or cracks (Sun et al., 2022). It is the reason that the proportions of air pores increased from 28 to 56 days for DW and SW-1.8% mixed samples. While, increasing salinity of seawater (from 0 to 3.6%) is conducive to inhibit the development of air pores or cracks (especially > 40 μm) in the samples as shown in Fig. 5(a).

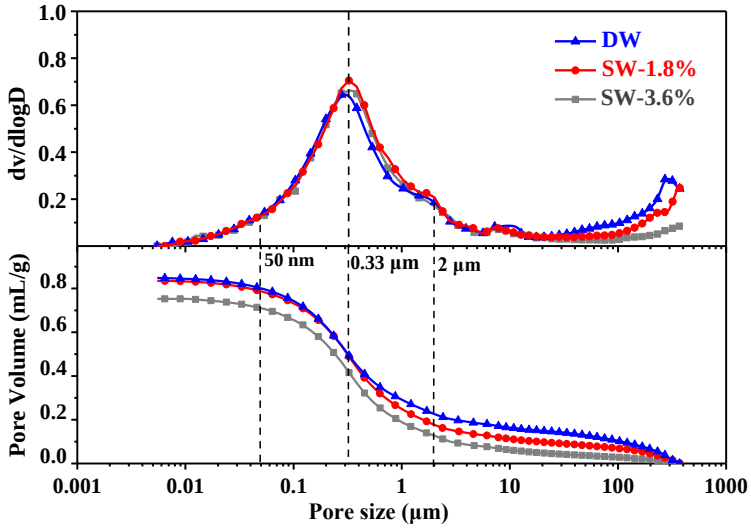

(a) PSD curves of treated HKMD from MIP method

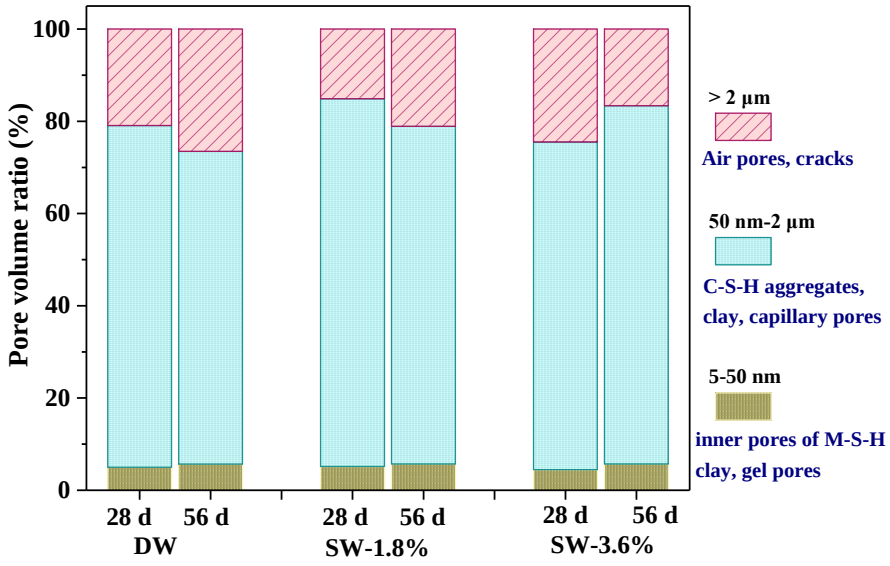

(b) Pore volume distribution of treated HKMD by MIP method.

Fig. 5. MIP results for the samples after 56 days curing.

3.4 NAI analysis

The PSD of the treated HKMD in powder state after 56 curing days was determined by NAI tests with the results compared in Fig. 6. The average pore diameter and BET SSA of the treated HKMD prepared by seawater with different levels of salinity are also determined. It is identified that the SSA value of the S/S HKMD powder increases with the salinity increasing, which is 15.99, 16.46, and 17.02 m^2/g under the conditions of DW, SW-1.8% and SW-3.6%, respectively. On the contrary, the average pore diameter of the treated HKMD decreases with the salinity increasing, which is 25.65, 24.59, and 23.25

nm under the conditions of DW, SW-1.8% and SW-3.6% (Sun et al., 2023b), respectively. It is reported that the development of surface area in cement pastes is dependent on highly porous phases, such as C-S-H (Garci Juenger and Jennings 2001; Thomas et al., 1999; Pan et al., 2015) and M-S-H (Bernard et al., 2019). Therefore, the improvement of SSA in the treated HKMD is mainly contributed to the development of C/M-S-H content. The results indicate that the treated HKMD sample with a 3.6% salinity of seawater exhibited the highest content of C/M-S-H phases, which agrees with the findings from TG analysis (see Table 5). The increasing quantity of C/M-S-H with salinity may be due to more Mg^{2+} in the SW (Garci Juenger and Jennings 2001).

The PSD of the S/S HKMD powders hydrated by three solutions is shown in Fig. 6. From Fig. 6(a), it is shown that the density of pores with diameter from 1.7-45 nm increases, and a peak at pore diameter of around 3 nm presents. The pore volume calculated from NAI data by using the BJH model increases in the treated HKMD in Fig. 6(b). It is also presented that the density of pores with diameter from 1.7-3 nm increases significantly, and then it almost keeps constant from 3-5 nm. The pore density of the 56-day sample mixed with SW of 3.6% salinity presents more nano pores. It can be inferred that the peak at 1.7 to 5 nm is contributed by the development of C/M-S-H phases (Pan et al., 2015). That means the increase of salinity promotes the hydration process in this work.

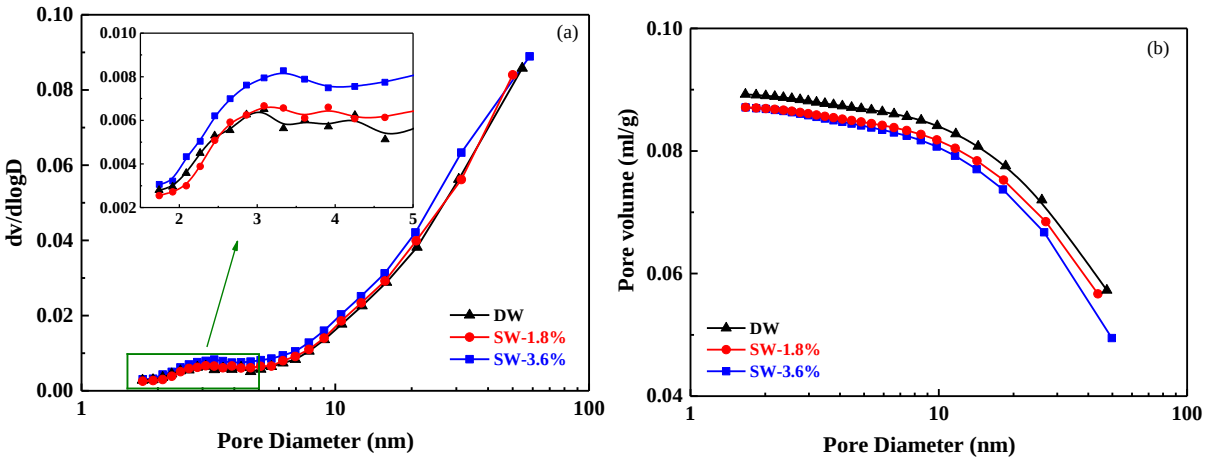

Fig. 6. The pore size distribution of treated HKMD powder at 56 curing days.

3.5 SEM-EDX analysis

3.5.1 Hydration products in the treated sample

The SEM photos of six types of hydration products or neoformation in the S/S HKMD samples with its element compositions analysed by EDS presented in Fig. 7. From Fig. 7(a), because the high content of Ca and around twice of O content, it is identified as $Ca(OH)_2$. In addition, the CH displays morphology of a multilayer flake aggregate. The new products with flocculent microstructure of light-colour are identified as C-S-H gels (see Fig. 7(b)). In Fig. 7(c), it was found a particle with the main element content of O, Si, Al, and Mg, which was considered for M-S-H gels. It is in agreement with the viewpoint of Tonelli et al. (2016) and Dewitte et al. (2022) that the M-S-H particles is homogeneous morphology and has the globular nature. It was also reported that CaO could react with Si and Al forming C-A-S-H gels (Hwang et al., 2014). Besides, the C-A-S-H can be formed from the pozzolanic reactions between kaolinite with CH in the mixture as well (Avet et al., 2019; Sun et al., 2023a). The EDS observations in this work confirm the products of C-(A)-S-H gels, ettringite, and F's salt in the treated HKMD samples. The fibrillar or needle-like morphology showing in Fig. 7(d) with the main element compositions of O, Si, Al, Ca and S is detected as AFt type phase (Bachtiar et al., 2022; Han et al., 2012). The square morphology coated by C-(A)-S-H is identified as F's salt, which is evident that most particles in the treated HKMD coated by new formatting gels. The AFt, F's salt and C-(A)-S-H integrate and attach to the other compositions in the system, which interlocks the particles and reinforces the structure of the S/S HKMD improving the strength and producing a lower porosity (Jha and Sivapullaiah, 2016; Yuan et al., 2009). In Fig. 7(f), the precipitated NaCl granule was found to be spherical in shape., which is confirmed by Zhang et al. (2022b) that in the kaolinite-based geopolymer system the presence of $MgCl_2$ induced halite formation.

The EDS result of the hydration products is mainly composed of Ca, Si, Al and O and other elements such as Na, S, Mg, Fe, Cl and K as well, which demonstrates that the EDS method can detect not only the target component, but also other products or compounds in the mixture (Sun et al., 2023a). In general, ions such as N, K, Mg and Fe presents in extremely low amounts but are negligible in the analysis (Rossen and Scrivener, 2017). According to the EDS data, some of the hydrations such as C-(A)-S-H, AFt phase and F's salt are mixed in Figs. 7(d) and 7(e). It is in agreement with that the C-A-S-H is often

used instead of C-S-H considering the incorporation of aluminum (Andersen et al., 2003; Avet et al., 2019).

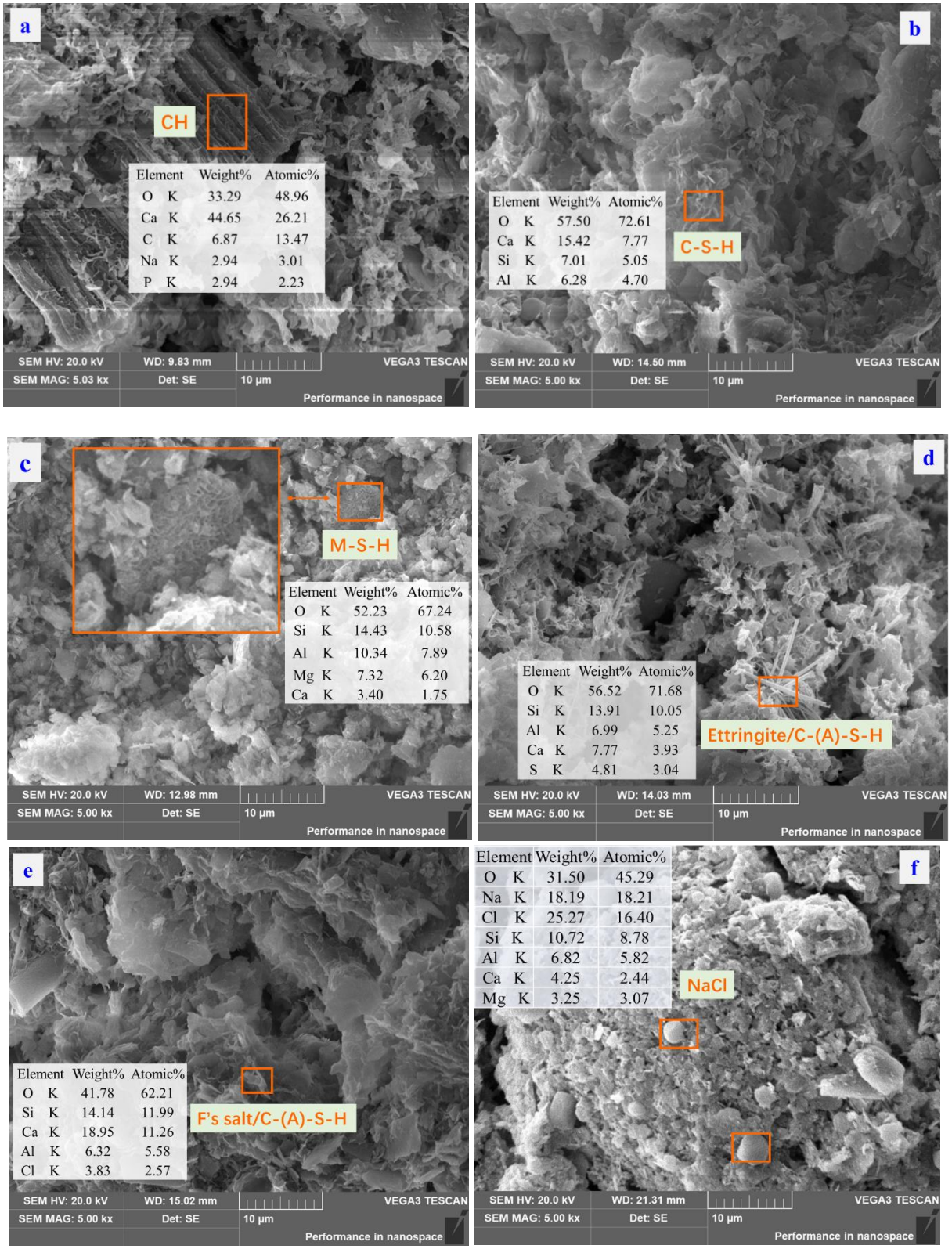

Fig. 7. SEM images of treated samples with different hydration products or neoformation.

3.5.2 Porosity analysis in the treated sample

Many cracks or air pores (> 2 μm) are observed as presenting on the SEM photos in Fig. 8(a). To analyse the porosity of cracks or air pores in S/S HKMD samples mixing with SW, ImageJ software was employed. To define and calculate the porosity, the gray value of the images was firstly extracted with the threshold gray of the cracks determined as shown in Figs. 8(a) and 8(b). Then, the porosity was calculated and shown in Fig. 8(c). The porosity of treated HKMD mixed with different salinity seawater was obtained from the average porosity in SEM images of various magnifications (from 1 kx to 10 kx), which is drawn in Fig. 8(d). It can be seen that the porosity of cracks (or air pores) in S/S samples after curing for 28 days decreases slightly with the salinity of substrate solution increasing and decreases significantly at 56 curing days. Therefore, increasing salinity of seawater (from 0 to 3.6%) is conducive to inhibit the development of cracks in the samples in this work. In addition, when the curing age increases from 28 to 56 days, the porosity of cracks increases. It is consistent with the results of the MIP test in Fig. 5.

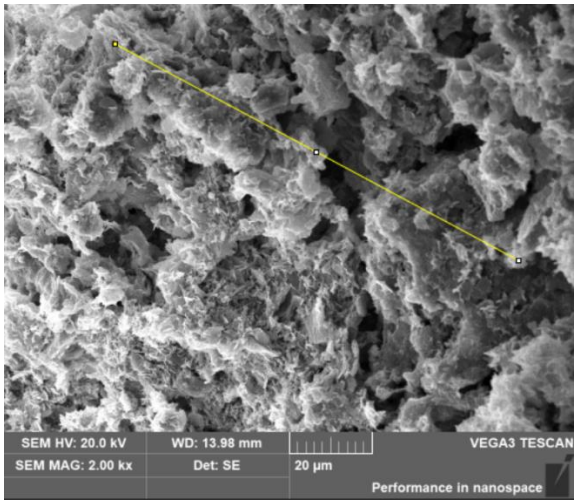

(a) SEM images of treated sample

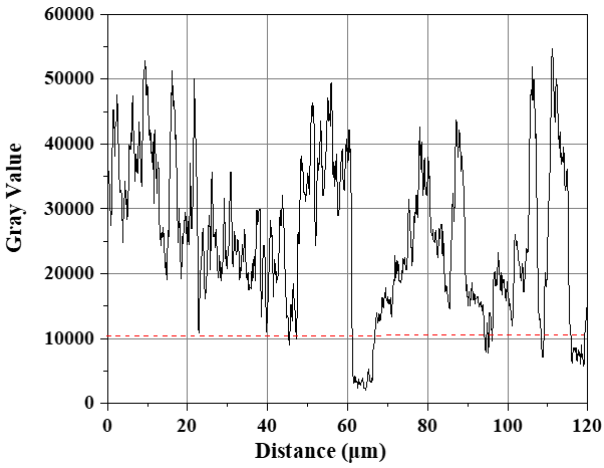

(b) Gray threshold for cracks

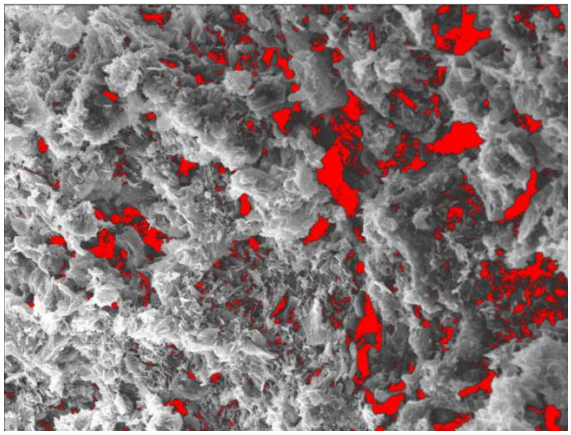

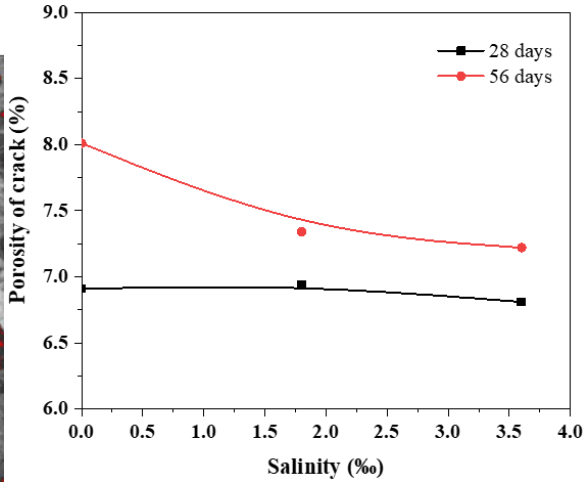

(c) Porosity determination (d) Porosity of cracks in S/S samples

Fig. 8. Porosity of cracks and air pores analysed by using ImageJ.

3.5.3 Statement of heavy metals in the treated sample

In addition to the main hydration products and marine deposit components, some organic matter, metallic minerals or some heavy metal elements are discovered by SEM-EDS test in both the block and powder S/S samples as shown in Fig. 9. The FeS_2 aggregate is found with the element compositions as shown in Fig. 9(a). It presents some small granular FeS_2, and its spherical aggregate has a diameter of 5-10 μm in Figs. 9(a) and 9(b). From Fig. 9(c), some ellipsoidal particles on the surface of the cube with long side around 29 μm are identified as ZrO_2 by EDS methods. In addition, an incomplete compact cube with a 39 mm long side was detected as TiO_2 in Fig. 9(d). As the basic compositions in the treated HKMD system are O, Si, Ca and Al, the EDS analysis of treated HKMD in powder state displays high intensity of these elements in Fig. 9(e-g). Apart from these elements, it is investigated that the elements such as Fe, Ni, Cu, Cr, Mo, Ti, etc., are also detected in the system coating by the other compounds, which suggests that the heavy metal (loid)s or toxic elements are well solidified and stabilized in the treated HKMD.

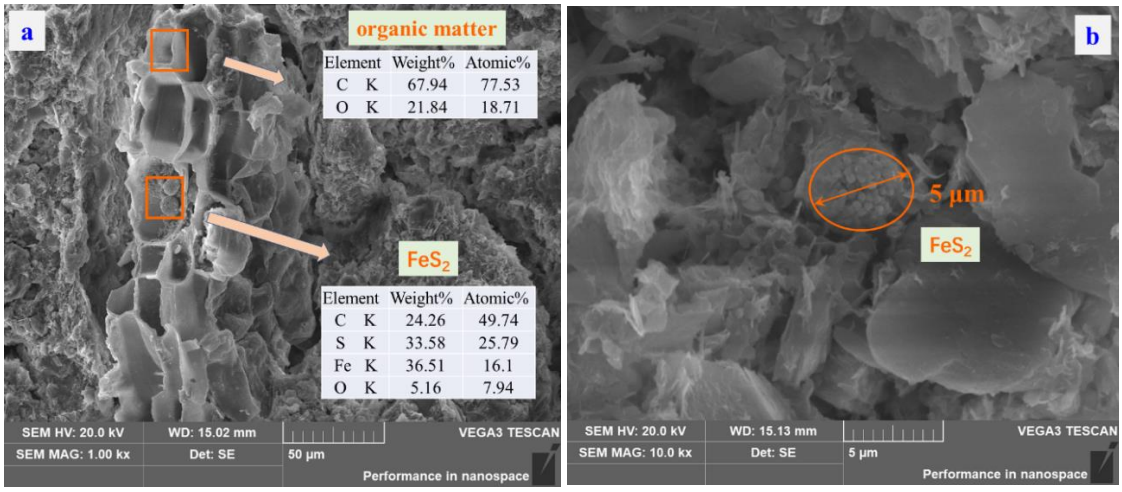

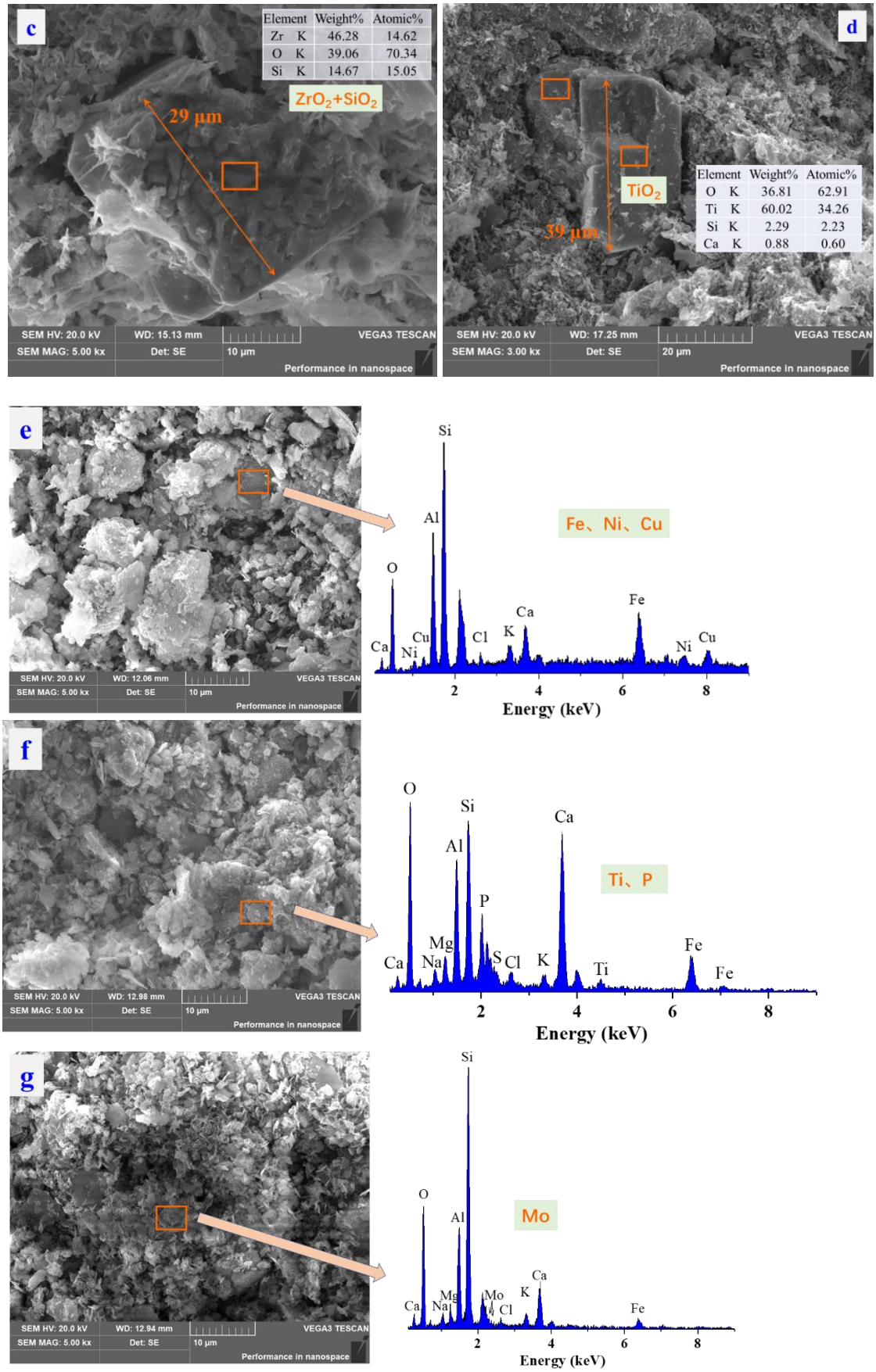

Fig. 9. SEM-EDS spectrum of the aggregation form of heavy metal-bearing minerals and minor elements in treated samples.

3.6 TCLP analysis

Because the deposits and industrial wastes contain a certain amount of metal(loid)s, the environmental risks of the S/S sediment materials are of great concern (Li et al. 2017). According to the TCLP test results, seven heavy metals from the lime-activated ISSA-GGBS treated Hong Kong marine deposits including As, Cd, Cr, Cu, Zn, Ni and Pb were analysed with the results shown in Fig. 10. As shown in Table 2, the theoretical leachability of Cd (0.30 mg/L), Cr (1.80 mg/L), Pb (1.07 mg/L), and Zn (6.56 mg/L) from the freshly mixed materials does not meet the reuse soil standard of Hong Kong (HK EPD 2011). Thus, the environmental risk of the cured soil should be evaluated before the engineering use. From Fig. 10, it is clear that all the leachability are environmentally acceptable with a low level of < 0.1 mg/L, which is far below the standard requirements of reuse treated soil (HK EPD, 2011). The results confirm that in this work the S/S process in the system could effectively stabilize the contaminants regardless of the curing time and the salinity of the mixing solution. Negligible toxic metals leaching from the S/S HKMD samples suggest that the lime-activated ISSA-GGBS treated Hong Kong marine deposits can be used for engineering applications directly without the leaching concerns.

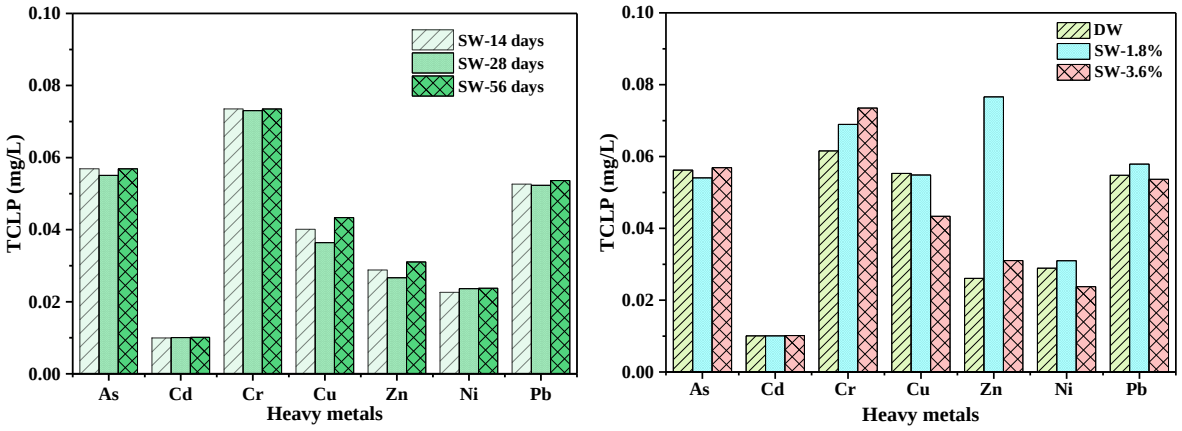

(a) Seawater at 3.6% salinity (b) Curing time of 56 days

Fig.10. Speciation of heavy metals in S/S treatment samples based on TCLP test.

4 Discussions

4.1 Seawater salinity effect on the porosity of treated soil

Pore structure is a main factor that affects the mechanical property of cement-based materials (Sun et al., 2022). The porosities of the S/S HKMD hydrated with seawater of different salinities were evaluated

from SEM observations and MIP methods with the result presented in Table 6. In order to intuitively understand the accuracy of the MIP testing results, the void ratio calculated ($e_{cal.}$) from water content and testing densities (see Section 3.1.1) are compared with the void ratio determined by MIP methods (e_{MIP}) in Table 6. It is obvious that $e_{cal.}$ is very stable with its value around 2. Taken $e_{cal.}$ as a reference value of theory void ratio, e_{MIP} are in its 90-107% range. Therefore, it can be thought that the MIP testing porosity of the treated HKMD is reasonable and credible in this work. It also means that the e_{MIP} of samples mixed with SW-1.8% at 28 curing days is smaller than the real one and that of samples with DW at 56 curing days is larger.

The porosity was evaluated from SEM observations by using imageJ software with the same method described in Section 3.5.2. Its value is statistically obtained after calculating and analysing SEM images with magnification from 1000 to 10000. From Table 6, it is observed that the average porosity is in the range of 50-65% and decreases with curing time, which is in consistent with the decreasing trend of void ratio in Fig. 2(b). It has been reported that AFt is the main products impacting the pore structure of S/S HKMD (Sun et al., 2023a). Thus, the decrease in porosity over time can be attributed to the increase content of AFt with time during the reaction processes in the system. From Table 6, which is obtained based on MIP test; the porosity is in the range of 60-70%, corresponding to the SEM results. According to the analysis, there are errors in the MIP test results, especially for samples mixed with SW-1.8% at 28 curing days and samples with DW at 56 curing days, so there is no clear decreasing trend over time. In addition, the minimum porosity is also found in the treated samples mixed with SW-1.8% from both methods. It is accepted that pore structure is one of the main factors affecting mechanical performance of cement-based materials because a lower porosity could enhance the strength of the block samples (Liu et al., 2019). Combing with the highest UCS and AFt content (see Fig. 4(a), Table 5), it can be concluded that it is feasible to use seawater in S/S treatment of HKMD, and the salinity of 1.8% is more conducive to improve its strength.

Besides the total void ratio and the statistical porosity, the crack porosity would also influence the properties of treated soil. In this work, the crack porosity estimated from SEM images decreases with the increasing of salinity from Fig. 8(d), which is confirmed by the MIP results in Fig. 5(a), especially for the pores with diameter > 40 μm. It also suggests that because of the lowest crack porosity the

intrusion pore volume of treated HKMD mixed with SW-3.6% is the smallest. Thus, higher salinity of seawater (0 - 3.6%) could inhibit the development of air pores or cracks in the S/S treated HKMD.

Table 6. Comparison of the void ratio and porosity calculated by different methods.

Conditions	e_{MIP}		$e_{cal.}$		Porosity-SEM (%)		Porosity-MIP (%)	
	28 days	56 days	28 days	56 days	28 days	56 days	28 days	56 days
DW	1.98	2.13	1.99	1.96	63.87	57.40	61.83	70.99
SW-1.8%	1.80	2.10	1.99	2.00	57.02	52.85	61.00	60.83
SW-3.6%	2.05	1.88	1.97	1.97	66.40	58.32	69.76	64.10

4.2 Seawater salinity effect on treated process

A mixture of multiple materials in the S/S HKMD makes the reactions within the system very complex. The basic reactions are the hydration and pozzolanic reactions. Among them, the hydration reactions include the hydration of lime and then the hydration of ISSA and GGBS under the alkaline conditions. The pozzolanic reactions involve the reaction of calcium hydroxide or magnesium hydroxide with clay minerals, in which clay minerals would provide amorphous silica or aluminum generating the products such as C/M-S-H, C-A-H or C-A-S-H (Gruyaert et al., 2012; Dauzeres et al., 2016).

It was pointed that many factors such as the clay content, organics, heavy metals, and salts contents in the sediment will affect the hydration process and strength development in the cement treated soil system (Wang et al., 2015). Additionally, the alkalinity of the mixture is also a key factor affecting the strength development of the treated clayey soil. A higher pH means a more alkaline environment, which is conducive to the hydration and pozzolanic reactions and thus the improvement of strength (Cai et al., 2022; Li and Yi, 2023). The pH of treated HKMD was measured by a pH meter with the dry soil/water ratio of 1:5 (GB LY/T 1251-199), which is 11.34, 11.38, and 11.31 under the conditions of DW, SW-1.8% and SW-3.6%, respectively. That is to say, the pH of treated HKMD with SW at 1.8% salinity is the highest. While the seawater was adopted as the mixed water, its main compositions (e.g., Na^+, Mg^{2+}, K^+, Cl^- and SO_4^{2-}) would have impacts on the reactions in the materials (Li et al., 2015). The presence of Mg^{2+}, Na^+ and K^+ in the seawater will result in the change of pH in the system due to the reactions as follows:

$$Mg^{2+} + Ca(OH)_2 \rightarrow Ca^{2+} + Mg(OH)_2 \downarrow \quad (1)$$

$$2Na^{+} + Ca(OH)_2 \rightarrow Ca^{2+} + 2NaOH \quad (2)$$

$$2K^{+} + Ca(OH)_2 \rightarrow Ca^{2+} + 2KOH \quad (3)$$

Where $Mg(OH)_2$ is less soluble than $Ca(OH)_2$, which causes a lower alkalinity in the mixture. On the contrary, NaOH and KOH will raise the alkalinity and thus the pH in the system.

According to Sun et al. (2023b), the strength of treated HKMD hydrated with $MgCl_2$ solution is the lowest because of Mg^{2+} reacting with OH^- forming $Mg(OH)_2$ and M-S-H phases (Sun et al., 2022), which has limited contribution in the strength improvement (Wang et al., 2019; Sun et al., 2023b). Besides, Song et al. (2023) reported that the strength of S/S marine deposits slurry by GGBS-MgO at the initial water content of 300% is lower than that by GGBS-CaO. The main reason may be that the pH of cases using GGBS-CaO is higher than that of cases using GGBS-MgO due to the difference between alkalinities of hydrated CaO and MgO (Jin and Al-Tabbaa, 2014). It was also confirmed by Zhang et al. (2022c) that the Na_2SiO_4-activated geopolymer exhibited a lower compressive strength after the addition of $MgCl_2$. Thus, the maximum Mg^{2+} in the system under the conditions of SW-3.6% can explain the lowest pH of treated soil in this case. Similarly, it can be deduced that under the conditions of SW-1.8% the positive impact of Na^+, K^+ on pH value is superior to the negative impact of Mg^{2+}, so the pH is highest, and the strength of the treated HKMD is the highest. The effect of seawater salinity on the soil system is the result of the synergistic action of the elements in seawater, especially the cations.

5 Conclusions

This study evaluated the stabilisation/solidification performance of HKMD mixed with seawater of different salinity from the aspects of engineering strength and environmental risk assessment. The lime-activated industrial wastes--ISSA and GGBS were adopted as binders. The following conclusions can be drawn:

1) Seawater could help S/S treated HKMD gain strength, and increasing the salinity of seawater is conducive to inhibit the development of cracks in the S/S samples.
2) Seawater of 1.8% salinity is better than distilled water and seawater of 3.6% salinity as a substrate solution in the S/S process, because of the highest UCS and lowest porosity in treated samples.

3) Based on the TCLP results, the S/S process could effectively stabilize the contaminants in the treated clayey soils with the leachates meeting the reuse standard in Hong Kong.

Therefore, this study proves that the S/S treated dredged clayey deposit by industrial wastes-ISSA and GGBS is technically feasible, economically sustainable and environmentally clean, which is possible to use it as geomaterials in reclamation projects.

Acknowledgements

This research was supported by the Research Grants Council of Hong Kong Special Administrative Region Government of China (Grant No.: R5037-18F and 15210322). The National Natural Science Foundation of China (Grant No.: 42125701) is greatly appreciated. The authors also acknowledge the financial supports from grants from Research Institute for Land and Space (CD7A and CD82) and Research Centre for Resources Engineering towards Carbon Neutrality (BBEJ) of Hong Kong Polytechnic University.

Declaration of interests

The authors declare that they have no known competing financial interests or personal relationships that could have appeared to influence the work reported in this paper.

Authors' contributions

Zhao SUN: Testing, analysis, investigation, and writing; **Wen-Bo CHEN**: Conceptualization, funding acquisition, review, and editing; **Run-Dong ZHAO**: Testing, and investigation; **Jiang-Shan LI and Zhenyu YIN**: Review and editing; **Jian-Hua YIN** and **Yong-Gui CHEN**: Supervision, project administration, review.

References

Alarcon-Ruiz, L., Platret, G., Massieu, E., Ehrlacher, A., 2005. The use of thermal analysis in assessing the effect of temperature on a cement paste. Cem. Concr. Res. 35 (3), 609–613.

Andersen, M.D., Jakobsen, H.J., Skibsted, J., Incorporation of aluminum in the calcium silicate hydrate (C-S-H) of hydrated Portland cements: a High-Field ^{27}Al and ^{29}Si MAS NMR investigation. Inorg. Chem. 42, 2280–2287.

Ashraf, W., Borno, I.B., Khan, R.I., Siddique, S., Haque, M.I., Tahsin, A., 2022. Mimicking the cementation mechanism of ancient Roman seawater concrete using calcined clays. Applied Clay Science 230, 106696.

Avet, F., Boehm-Courjault, E., Scrivener, K., 2019. Investigation of C-A-S-H composition, morphology and density in Limestone Calcined Clay Cement (LC3). Cement and Concrete Research 115, 70–79.

Avet, F., Scrivener, K., 2018. Investigation of the calcined kaolinite content on the hydration of Limestone Calcined Clay Cement (LC3). Cement and Concrete Research 107, 124–135.

Bachtiar, E., Rachim, F., Makbul, R., Tata, A., Irfan-Ul-Hassan, M., Kırgız, M. S., Syarif, M., de Sousa Galdino, A. G., Khitab, A., Benjeddou, O., Kolovos, K. G., Ledesma, E. F., Yusri, A., Papatzani, S., 2022. Monitoring of chloride and Friedel's salt, hydration components, and porosity in high-performance concrete. Case Studies in Construction Materials 17, e01208.

Bernard, E., Lothenbach, B., Le Goff, F., Pochard, I., Dauzères, A., 2017. Effect of magnesium on calcium silicate hydrate (C-S-H). Cement and Concrete Research 97, 61–72.

Bernard, E., Lothenbach, B., Chlique, C., Wyrzykowski, M., Dauzères, A., Pochard, I.8, Cau-Dit-Coumes, C., 2019. Characterization of magnesium silicate hydrate (M-S-H). Cement and Concrete Research 116, 309–330.

Cai, G.H. Zhou, Y.F., Poon, C.S., Li, J.S., 2022. Engineering performance and microstructure characteristics of natural marine sediment stabilized with quicklime-activated GGBS under different lime proportions, Marine Georesources & Geotechnology 1–15.

Castaldi, P., Santona, L., Melis, P., 2005. Heavy metal immobilization by chemical amendments in a polluted soil and influence on white lupin growth. Chemosphere 60, 365-371.

Celik, E., Nalbantoglu, Z., 2013. Effects of ground granulated blastfurnace slag (GGBS) on the swelling properties of lime-stabilized sulfate-bearing soils. Engineering Geology 163, 20–25.

Chakraborty, S., Puppala, A.J., Biswas, N., 2022. Role of crystalline silica admixture in mitigating ettringite-induced heavein lime-treated sulfate-rich soils. Géotechnique 72 (5), 438–454.

Chiang, W.S., Ferraro, G., Fratini, E., Ridi, F., Yeh, Y.Q., Jeng, U.S., Chen, S.H., Baglioni, P., 2014. Multiscale structure of calcium- and magnesium-silicate-hydrate gels. Journal of Materials Chemistry A 2, 12991.

Chen, L., Lin, D.F., 2009. Stabilization treatment of soft subgrade soil by sewage sludge ash and cement. J. Hazard Mater. 162, 321–327.

Chen, L., Wang, Y.S., Wang, L., Zhang, Y., Li,J., Tong, L., Hu, Q., Dai, J.G., Tsang, D.C.W., 2021. Stabilisation/solidification of municipal solid waste incineration fly ash by phosphate-enhanced calcium aluminate cement. J Hazard Mater 408, 124404.

Dauzeres, A., Achiedo, G., Nied, D., Bernard, E., Alahrache, S., Lothenbach, B., 2016. Magnesium perturbation in low-pH concretes placed in clayey environment–solid characterizations and modeling. Cem. Concr. Res. 79, 137–150.

Deng, Y., Yue, X., Liu, S., Chen, Y., Zhang, D., 2015. Hydraulic conductivity of cement-stabilized marine clay with metakaolin and its correlation with pore size distribution. Engineering Geology 193, 146-152.

Deng, Y., Zhang, T., Cui, Y., Chen, Y., Deng, T., Zhou, X., 2018. Pore water salinity effect on the intrinsic compression behaviour of artificial soft soils. Applied Clay Science 166, 299-306.

Dewitte, C., Bertron, A., Neji, M., Lacarriere, L., Dauzeres, A., 2022. Chemical and Microstructural Properties of Designed Cohesive M-S-H Pastes. Materials 15 (2), 547.

Emmanuel, E., Yong, L. L., Anggraini, V., Pasbakhsh, P., 2020. Can halloysite nanotubes be used to remediate zinc and lead-contaminated marine clay? A solidification/stabilization approach: Applied Clay Science 186.

Gallucci, E., Zhang, X., Scrivener, K. L., 2013. Effect of temperature on the microstructure of calcium silicate hydrate (C-S-H). Cement and Concrete Research 53, 185–195.

Garci Juenger, M.C., Jennings, H.M., 2001. The use of nitrogen adsorption to assess the microstructure of cement paste. Cem. Concr. Res. 31 (6), 883–892.
Gruyaert, E., Van Den Heede, P., Maes, M., De Belie, N., 2012. Investigation of the influence of blast-furnace slag on the resistance of concrete against organic acid or sulphate attack by means of accelerated degradation tests. Cem. Concr. Res. 42, 173–185.
Gong, L., Wang, J., Abbas, T., Zhang, Q., Cai, M., Tahir, M., Wu, D., Di, H., 2021. Immobilization of exchangeable Cd in soil using mixed amendment and its effect on soil microbial communities under paddy upland rotation system. Chemosphere 262, 127828.
Han, S., Yan, P., Liu, R., 2012. Study on the hydration product of cement in early age using TEM. Science China Technological Sciences 55 (8), 2284–2290.
HK CEDD, 2017. Model Specification for Soil Testing, Geospec3. Geotechnical Engineering Office. Civil Engineering and Development Department. https://www.cedd.gov.hk/filemanager /eng/content_122/es3_20170829.pdf.
HK EPD, 2011. Practice guide for investigation and remediation of contaminated land. Environmental Protection Department, Hong Kong SAR Government.
Horpibulsuk, S., Rachan, R., Raksachon, Y., 2009. Role of Fly Ash on Strength and Microstructure Development in Blended Cement Stabilized Silty Clay. Soils and Foundations 49 (1), 85–98.
Horpibulsuk, S., Rachan, R., Chinkulkijniwat, A., Raksachon, Y., Suddeepong, A., 2010. Analysis of strength development in cement-stabilized silty clay from microstructural considerations. Constr. Build. Mater. 24 (10), 2011–2021,
Horpibulsuk, S., Phojan, W., Suddeepong, A., Chinkulkijniwat, A., Liu, M. D., 2012. Strength development in blended cement admixed saline clay. Applied Clay Science 55, 44-52.
Huang, Y., Wang, L., Wang, W., Li, T., He, Z., Yang, X., 2019. Current status of agricultural soil pollution by heavy metals in China: a meta-analysis. Sci. Total Environ. 651, 3034–3042.
Húlan, T., Trník, A., Štubňa, I., Bačík, P., Kaljuvee, T., Vozár, L., 2015. Thermomechanical Analysis of Illite from FÜzÉrradvÁny. Materials Science 21, 3.
Hwang, K.Y., Seo, J.Y., Phan, H.Q., Ahn, J.Y., Hwang, I., 2014. MgO-based binder for treating contaminated sediments: Characteristics of metal stabilization and mineral carbonation. CLEAN–Soil, Air, Water 42 (3), 355–363.
Jagaba, A.H., Shuaibu, A., Musa, S., Lawal, I.M., Abubakar, S., 2019. Stabilization of soft soil by incinerated sewage sludge ash from municipal wastewater treatment. Plant for Engineering Construction 2, 32–44.
Jha, A.K., Sivapullaiah, P.V., 2016. Volume change behavior of lime treated gypseous soil— influence of mineralogy and microstructure. Applied Clay Science 119, 202–212.
Jin, F., Al-Tabbaa, A., 2014. Characterisation of different commercial reactive magnesia. Adv. Cement Res. 26 (2), 101–113.Jin, F., Wang, F., Al-Tabbaa, A., 2016. Three-year performance of in-situ solidified/ stabilized soil using novel MgO-bearing binders, Chemosphere 144, 681–688.
Khoshsirat, V., Bayesteh, H., Sharifi, M., 2019. Effect of high salinity in grout on the performance of cement-stabilized marine clay. Construction and Building Materials 217, 93–107.
Lang, L., Chen, B., Chen, B., 2021. Strength evolutions of varying water content-dredged sludge stabilized with alkali-activated ground granulated blast-furnace slag. Construction and Building Materials 275, 122111.
Li, J.S., Wang, L., Tsang, D.C., Beiyuan, J., Poon, C.S., 2017. Dynamic leaching behavior of geogenic as in soils after cement-based stabilization/solidification. Environ. Sci. Pollut. Res. 24 (36), 27822–27832.
Li, J.S., Zhou, Y.F., Wang, Q.M., Xue, Q., Poon, C.S., 2019. Development of a Novel Binder Using Lime and Incinerated Sewage Sludge Ash to Stabilize and Solidify Contaminated Marine Sediments with High Water Content as a Fill Material. Journal of Materials in Civil Engineering 31(10), 04019245.
Li, Q., Geng, H., Shui, Z., Huang, Y., 2015. Effect of metakaolin addition and seawater mixing on the properties and hydration of concrete. Applied Clay Science 115, 51–60.
Li, W., Yi, Y., Puppala, A. J., 2022. Comparing carbide sludge-ground granulated blastfurnace slag and ordinary Portland cement: Different findings from binder paste and stabilized clay slurry. Construction and Building Materials 321, 126382.
Li, W., Yi, Y., 2023. Estimating the Optimum Addition of Carbide Sludge for Enhancing Strength Development of Ground-Granulated Blast Furnace Slag-Treated Slurry Based on Initial pH. Journal of Materials in Civil Engineering 35(2), 04022400.

Lofrano, G., Libralato, G., Minetto, D., De Gisi, S., Todaro, F., Conte, B., Calabro, D., Quatraro, L., Notarnicola, M., 2017. In situ remediation of contaminated marinesediment: an overview. Environ Sci Pollut Res Int 24(6), 5189–5206.

Lu, J.X., Poon, C.S., 2018. Improvement of early-age properties for glass-cement mortar by adding nanosilica. Cement Concr. Compos. 89, 18–30.

Malviya, R., Chaudhary, R., 2006. Leaching behavior and immobilization of heavy metals in solidified/stabilized products. J Hazard Mater 137(1), 207–217.

Min, X.B., Liu, D.G., Chai, L.Y., Ke, Y., Liang, Y.J., Shi, M.Q., Li, Y.C., Tang, C.J., Wang, Y.Y., Wang, Z.B., 2019. Comparison of arsenic immobilization properties among calcium silicate hydrate, ettringite, and friedel's salt in a slag-based binder. Environmental Progress & Sustainable Energy 38(S1), S422–S428.

Monsif, M. Y., Liu, J., Gurpersaud, N., 2020. Impact of salinity on strength and microstructure of cement-treated Champlain Sea clay. Marine Georesources & Geotechnology39(11), 1360–1372.

Nied, D., Enemark-Rasmussen, K., L'Hopital, E., Skibsted, J., Lothenbach, B., 2016. Properties of magnesium silicate hydrates (M-S-H). Cement and Concrete Research 79, 323–332.

Pan, Z., He, L., Qiu, L., Korayem, A.H., Li, G., Zhu, J.W., Collins, F., Li, D., Duan, W. H., Wang, M.C., 2015. Mechanical properties and microstructure of a graphene oxide–cement composite. Cement and Concrete Composites 58, 140–147.

Prochon, P., Piotrowski, T., 2020. The effect of cement and aggregate type and w/c ratio on the bound water content and neutron shielding efficiency of concretes. Construction and Building Materials 264, 120210.

Rossen, J. E., Scrivener, K. L., 2017. Optimization of SEM-EDS to determine the C–A–S–H composition in matured cement paste samples. Materials Characterization 123, 294–306.

Scrivener, K., Snellings, R., Lothenbach, B., 2017. A Practical Guide to Microstructural Analysis of Cementitious Materials. Taylor & Francis Group.

Singh, A., Agrawal, M., Marshall, F.M., 2010. The role of organic vs. inorganic fertilizers in reducing phytoavailability of heavy metals in a wastewater-irrigated area. Ecological Engineering 36(12), 1733–1740.

Shen, P., Lu, L., He, Y., Wang, F., Hu, S., 2017. Hydration of quaternary phase-gypsum system. Constr. Build. Mater. 152, 145–153.

Song, D.B., Chen, W.B., Yin, Z.Y., Shi, X.S., Yin, J.H., 2023. Recycling dredged mud slurry using vacuum-solidification combined method with sustainable alkali-activated binder: Geotextiles and Geomembranes. https://doi.org/10.1016/j.geotexmem.2023.05.003

Song, M.M., Zeng, L.L., Hong, Z.S., 2017. Pore fluid salinity effects on physicochemical-compressive behaviour of reconstituted marine clays. Applied Clay Science 146, 270-277.

Sun, Y., Lu, J.X., Poon, C.S., 2022. Strength degradation of seawater-mixed alite pastes: an explanation from statistical nanoindentation perspective. Cement and Concrete Research 152, 106669.

Sun, Z., Chen, Y.G., Ye, W.M., Cui, Y.J., Wang, Q., 2020. Swelling deformation of Gaomiaozi bentonite under alkaline chemical conditions in a repository. Engineering Geology 279, 105891.

Sun, Z., Chen, W.B., Zhao, R.D., Jin, Y.F., Yin, J.H., 2023a. Solidification/stabilization treatment of Hong Kong marine deposits slurry at high water content by ISSA and GGBS. Construction and Building Materials 372, 130817.

Sun, Z., Chen, W.B., Zhao, R.D., Shen, P., Yin, J.H., Chen, Y.G., 2023b. Effect of seawater on solidification/stabilisation treatment of marine soft soil slurry by lime-activated ISSA and GGBS. Engineering Geology 323, 107216.

Tonelli, M., Martini, F., Calucci, L., Fratini, E., Geppi, M., Ridi, F., Borsacchi, S., Baglioni, P., 2016. Structural Characterization of Magnesium Silicate Hydrate: Towards the Design of Eco-Sustainable Cements. Dalton Trans. 45, 3294–3304.

Thomas, J.J., Jennings, H.M., Allen, A.J., 1999. The Surface Area of Hardened Cement Paste as Measured by Various Techniques. Concr. Sci. Eng. 1 (1), 45–64.

US EPA 1311, 1992. Toxicity Characteristic Leaching Procedure. US Environ. Prot. Agency, Washington, DC, USA.

Wang, K., Shah, S.P., Mishulovich, A., 2004. Effects of curing temperature and NaOH addition on hydration and strength development of clinker-free CKD-fly ash binders, Cem Concr Res. 34 (2), 299–309.

Wang, L., Kwok, J.S.H., Tsang, D.C.W., Poon, C.S., 2015. Mixture design and treatment methods for recycling contaminated sediment. J. Hazard Mater. 283, 623–632.

Wang, L., Chen, L., Cho, D. W., Tsang, D. C. W., Yang, J., Hou, D., Baek, K., Kua, H. W., Poon, C. S., 2019. Novel synergy of Si-rich minerals and reactive MgO for stabilisation/solidification of contaminated sediment. J Hazard Mater 365, 695–706.

Wu, H.L., Jin, F., Bo, Y.L., Du, Y.J., Zheng, J.X., 2018. Leaching and microstructural properties of lead contaminated kaolin stabilized by GGBS-MgO in semi-dynamic leaching tests. Construction and Building Materials 172, 626–634.

Xu, D.M., Fu, R.B., Wang, J.X., Shi, Y.X., Guo, X.P., 2021. Chemical stabilization remediation for heavy metals in contaminated soils on the latest decade: Available stabilizing materials and associated evaluation methods—A critical review. Journal of Cleaner Production 321, 128730.

Yi, Y.L., Gu, L.Y., Liu, S., 2015. Microstructural and mechanical properties of marine soft clay stabilized by lime-activated ground granulated blastfurnace slag. Applied Clay Science 103, 71–76.

Yu, C.Y., Chow, J.K., Wang, Y.H., 2016. Pore-size changes and responses of kaolinite with different structures subject to consolidation and shearing. Engineering Geology 202, 122–131.

Yuan, Q., Shi, C., De Schutter, G., Audenaert, K., Deng, D., 2009. Chloride binding of cement-based materials subjected to external chloride environment – a review. Construct. Build. Mater. 23 (1), 1–13.

Zeng, Q., Li, K.F., Chong, T.F., Dangla, P., 2012. Pore structure characterization of cement pastes blended with high-volume fly-ash. Cem. Concr. Res. 42, 194–204.

Zentar, R., Wang, D., Abriak, N.E., Benzerzour, M., Chen, W., 2012. Utilization of siliceous–aluminous fly ash and cement for solidification of marine sediments. Construct. Build. Mater. 35, 856–863.

Zhang, D., Cao, Z., Fan, L., Liu, S., Liu, W., 2014. Evaluation of the influence of salt concentration on cement stabilized clay by electrical resistivity measurement method. Engineering Geology 170, 80–88.

Zhang, B., Yu, T., Deng, L., Li, Y., Guo, H., Zhou, J., Li, L., Peng, Y., 2022a. Ion-adsorption type rare earth tailings for preparation of alkali-based geopolymer with capacity for heavy metals immobilization. Cement and Concrete Composites 134, 104768.

Zhang, B., Huang, D., Li, L., Lin, M., Liu, Y., Fang, W., Lu, J., Liu, F., Li, Y., Liu, Y., Xiong, Z., 2022b. Effect of magnesium salt contamination on the microstructures and properties of metakaolinite-based geopolymer: the role of $MgCl_2$ and $MgSO_4$. Journal of Materials Research and Technology 20, 4500–4514.

Zhang, K., Wang, K., Liu, Z., Ye, Z., Zhang, B., Lu, D., Liu, Y., Li, L., Xiong, Z., 2022c. Effect of Magnesium Salt ($MgCl_2$ and $MgSO_4$) on the Microstructures and Properties of Ground Granulated Blast Furnace Slag (GGBFS)-Based Geopolymer. Materials 15, 4911.

Zhao, Y., Hu, X., Shi, C., Zhang, Z., Zhu, D., 2021. A review on seawater sea-sand concrete: Mixture proportion, hydration, microstructure and properties. Construction and Building Materials 295, 123602.

Zhou, Y., Li, J., Lu, J., Cheeseman, C., Poon, C.S., 2020. Sewage sludge ash: a comparative evaluation with fly ash for potential use as lime-pozzolan binders. Construct. Build. Mater. 242, 118160.

Zhou, Y., Lu, J., Li, J., Cheeseman, C., Poon, C.S., 2021a. Hydration, mechanical properties and microstructure of lime-pozzolana pastes by recycling waste sludge ash under marine environment. Journal of Cleaner Production 310, 127441.

Zhou, Y., Lu, J., Li, J., Cheeseman, C., Poon, C.S., 2021b. Influence of seawater on the mechanical and microstructural properties of lime-incineration sewage sludge ash pastes. Construction and Building Materials 278, 122364.

Zhou, Y., Cai, G., Cheeseman, C., Li, J., Poon, C.S., 2022. Sewage sludge ash-incorporated stabilisation/solidification for recycling and remediation of marine sediments. J Environ Manage 301, 113877.